LAWRENCE
LIVERMORE
NATIONAL
LABORATORY

LLNL-JRNL-769201

Creation of well-defined "mid-sized" micropores in carbon molecular sieve membranes

Y. Ma, M. L. Jue, F. Zhang, R. Mathias, H. Jang, R. P. Lively

March 8, 2019

Angewandte Chemie International Edition

Creation of well-defined "mid-sized" micropores in carbon molecular sieve membranes

Yao Ma, Melinda L. Jue, Fengyi Zhang, Ronita Mathias, Hye Youn Jang, and Ryan P. Lively*

Abstract: Carbon molecular sieve (CMS) membranes are candidates for the separation of organic molecules due to their stability, ability to be scaled at practical form factors, and the avoidance of expensive supports or complex multi-step fabrication processes. A critical challenge is the creation of "mid-range" (e.g., 5-9 Å) microstructures that allow for facile permeation of organic solvents and selection between similarly-sized guest molecules. Here, we create these microstructures via the pyrolysis of a microporous polymer (PIM-1) under low concentrations of hydrogen gas. The introduction of H_2 inhibits aromatization of the decomposing polymer and ultimately results in the creation of a well-defined bimodal pore network that exhibits an ultramicropore size of 5.1 Å. The H_2-assisted CMS dense membranes show a dramatic increase in *p*-xylene ideal permeability (~15 times), with little loss in *p*-xylene/*o*-xylene selectivity (18.8 vs. 25.0) when compared to PIM-1 membranes pyrolyzed under a pure argon atmosphere. This approach is successfully extended to hollow fiber membranes operating in organic solvent reverse osmosis mode, highlighting the potential of this approach to be translated from the laboratory to the field.

Bulk and specialty chemical production are founded on organic syntheses, which ultimately require purification or separation of organic mixtures to obtain desired product purities or recoveries.[1] An important example of organic solvent separations is the purification of benzene derivatives, particularly xylene isomers, which are of significant importance in the petrochemical industry for the production of chemicals such as polyethylene terephthalate, isophthalic acid, and phthalic anhydride.[2] Compared to the conventional techniques such as simulated moving bed and fractional crystallization, membrane-based approaches provide an attractive supplement or even alternative to these techniques, as there is the potential to improve energy efficiency, improve productivity, reduce operational complexity, and reduce capital costs.[3]

Polycrystalline zeolite MFI-type membranes have been widely studied in the field of xylene isomers separations, typically using pervaporation or vapor permeation separation modalities.[4] However, the MFI framework can undergo structural distortions upon the adsorption of xylene molecules, especially near ambient temperatures and at high xylene loadings. This distortion can induce the phase change of the MFI crystals from an orthorhombic phase (ORTHO) to a second orthorhombic phase (PARA) that renders the structures unable to distinguish between the xylene isomers and reduces the separation efficiency of the membrane.[5] This issue, coupled with low xylene permeances at high fractional occupancies of the guest molecule, suggests that MFI-type zeolite membranes will struggle to provide satisfactory xylene isomer separation at industrially-relevant conditions. Moreover, the requirement of expensive supports and the difficulty of scale-up production acts as further deterrents to the practical application of MFI membranes for xylene separations despite their exceptional performance in the lab. As the demand of xylene isomers is expected to maintain a 5-7% yearly growth,[6] it is imperative to develop new, scalable membranes that exhibit promising separation performance under practical operating conditions.

Carbon molecular sieve (CMS) membranes, formed via the pyrolytic decomposition of polymeric materials, are solvent- and temperature-resistant materials that have the ability to withstand high transmembrane pressures when fabricated into the form of hollow fibers.[7] Hollow fibers can be fabricated as "asymmetric membranes", which have a thin separating layer that provides mechanical support and transitions to a more porous substructure. Typically, this membrane asymmetry is created during a single-step phase inversion process. An asymmetric structure is critical for enabling high product permeances while providing mechanical integrity to the membrane. A recent report from our group has shown that asymmetric CMS hollow fiber membranes derived from cross-linked polyvinylidene fluoride have the ability to separate xylene isomers in a separation modality known as "organic solvent reverse osmosis" (OSRO).[8] The cross-linking process critical for maintaining the membrane asymmetry adds several additional fabrication steps, thus increasing the cost and complexity associated with creating these materials at scale. Polymers of intrinsic microporosity (e.g., PIM-1) have drawn attention as polymeric precursors for the fabrication of CMS materials due to their high glass transition temperature, which has been shown to be a critical property in the maintenance of an asymmetric membrane structure during pyrolysis.[9] Specifically, if the glass transition temperature (442 °C for PIM-1) is above the polymer decomposition temperature (~415 °C for PIM-1), the membrane asymmetry will be retained throughout pyrolysis, as the polymer precursor will remain in the glassy state until the degradation process begins.[10]

Previous work on "dense" CMS films prepared from PIM-1 precursors has shown that these materials have competitive xylene permeabilities and entropy-dominated selectivities for the para-/ortho- isomer pair.[11] Importantly, these performance parameters were achieved under conditions of high guest molecule fractional occupancy in the membrane. However, the size of the ultramicropores inside this kind of CMS material is quite similar to N_2 (3.64 Å), which severely limits the transport rate of *p*-xylene.[11] Various templating and block copolymer techniques are able to create well-defined carbonaceous pores in

Y. Ma, Dr. M. L. Jue, F. Zhang, R. Mathias, H. Jang, Prof. R. P. Lively
School of Chemical & Biomolecular Engineering
Georgia Institute of Technology
311 Ferst Drive NW, Atlanta, Georgia 30332, United States
E-mail: ryan.lively@chbe.gatech.edu

Supporting information for this article is given via a link at the end of the document.

the range of 1-2 nm[12] and pyrolysis of high free volume polyimides is capable of creating CMS materials with pores less than 0.5 nm.[13] However, the creation of well-defined micropores in the range of 0.5-1 nm is difficult, and existing techniques require complex precursor pretreatments or extensive chemical post-treatments on the as-made CMS membranes. Kim et al. fabricated carbonaceous membranes for water treatment by heating PIM-1 in an N_2/H_2 gas (95/5 vol%) environment (1100-1300 °C at 5 °C min^{-1}); however, these authors observed a carbon pore structure with a wide distribution of pores.[14] Inspired by this work and the teachings from the pyrolysis of high free volume polyimides, we create "mid-range" micropores in CMS membranes via incorporation of H_2 in our pyrolysis environment, but utilize a heating protocol designed for the fabrication of well-defined CMS structures. Moreover, we show that this approach can be easily applied to create hollow fiber membranes capable of separating xylene isomers.

The fluorescent yellow PIM-1 polymer was produced from the reaction of tetrafluoroterephthalonitrile (TFTPN) and 5,5',6,6'-tetrahydroxy- 3,3,3',3'-tetramethyl-1,1'-spirobisindane (TTSBI) in dimethylformamide.[15] Freestanding dense PIM-1 films were prepared from PIM-1/tetrahydrofuran solution casting while the asymmetric PIM-1 hollow fiber membranes (HFM) were spun using a simulated dual-bath method as described previously.[16] Afterward, the PIM-1 was pyrolyzed in a controlled environment to create the CMS. The final pyrolysis temperature (500, 800, or 1100 °C) was controlled via a three-zone tube furnace while the H_2 concentration (4, 2, 1, or 0 vol%) was tuned by combining a premixed 4 vol% H_2/Ar and a UHP Ar stream at the appropriate flow rate ratios (**Figure 1**). It is important to note that 4 vol% is the lower explosive limit of hydrogen in air at ambient temperature and pressure;[17] we elected to use vendor-mixed tanks of H_2/Ar to stay below this limit and then further dilute this tank with pure argon to tune the hydrogen concentration. The resulting dense membrane samples were named with the final pyrolysis temperature and H_2 concentration. For example, "CMS_500 °C_4% H_2" indicates a dense CMS membrane fabricated at 500 °C in a 4 vol% H_2 atmosphere. The CMS hollow fiber membranes were fabricated only at 500 °C and are named according to their H_2 concentration such as "CMS_HFM_4% H_2". The details of the experimental method related to the fabrication of CMS membranes can be found in the Supporting Information.

The evolution of the CMS microstructure during the pyrolysis of polyimides has been investigated in detail by Rungta et al.[18] Although CMS materials formed from various polymer precursors are likely to be different in final structure and performance, the general evolution of the CMS structure should be qualitatively similar for all precursors of a similar class (e.g., high free volume, linear, glassy polymers). In a typical pyrolysis protocol for CMS membranes (as represented in Supporting Information **Table S1** with three distinct periods: ramp, soak, and cool), PIM-1 will evolve from a random polymer coil to an amorphous, isotropic, and microporous CMS material as illustrated in **Figure S1**.[18a] The enlargement of ultramicropores due to the introduction of H_2 is illustrated in **Figure 2a** and can be explained by investigating the transition of the PIM-1 coils to CMS.

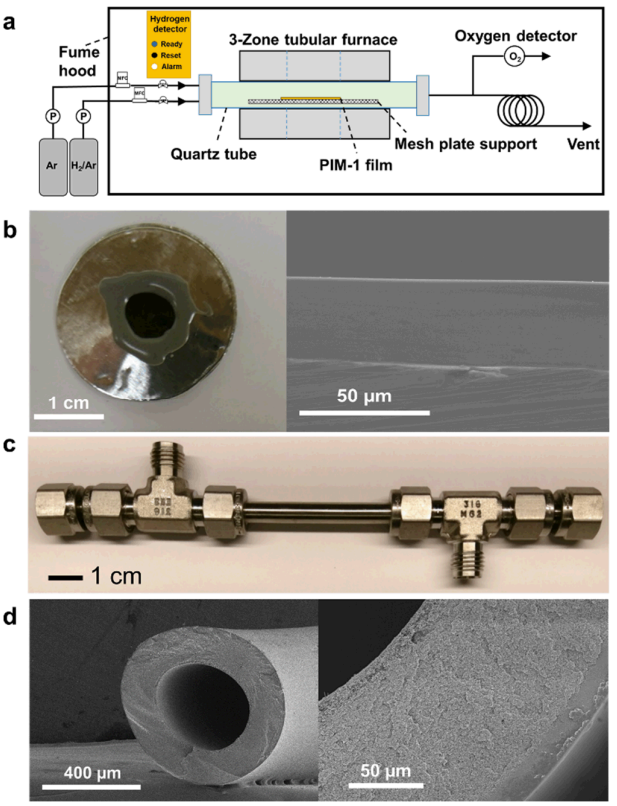

Figure 1. a) Diagram of the pyrolysis setup. b) Left: digital photograph of a PIM-1-derived CMS dense membrane sealed with epoxy and aluminium tape for permeation testing; Right: the SEM cross-sectional image of a CMS dense membrane. c) Digital photograph of a CMS HFM module. d) SEM cross-sectional images of a CMS HFM.

Initially, in the thermal ramp process, the entangled semi-flexible PIM-1 precursor (**Figure S1(i)**) undergoing aromatization and fragmentation will tend to experience sufficient localized stresses such that periodic scissions along the polymer backbone occur. Such backbone scissions generate CO_2 and H_2O that remove most of the oxygen atoms in PIM-1, resulting in potentially rigid, highly aromatic strands (**Figure S1(ii)**). Based on the amount of evolved CO_2 and H_2O during pyrolysis as measured by off-gas mass spectrometry (**Figure 2b** and Supporting Information **Figure S2**) and sp^3/sp^2 carbon ratio measured by X-ray photoelectron spectroscopy, hypothetical reaction pathways for this process are proposed (**Figure 2c**). The generated reaction products will then connect with each other to form the rigid strands. The existence of H_2 in the pyrolysis environment will inhibit the loss of oxygen in the form of CO_2 (as shown in idealized pyrolysis reaction 1) and promote the removal of oxygen atoms in the form of H_2O (as shown in idealized pyrolysis reactions 2 and 3). As compared to the inert pyrolysis case, the evolved gases from the H_2-included pyrolysis show a substantial reduction in the evolution of CO_2 and a significant increase in the production of H_2O (**Figure 2b**). As a result, the strands formed in the H_2-included pyrolysis environment will be more kinked compared to those formed in pure Ar, since the conversion of PIM-1 units to relatively twisted units (products of idealized pyrolysis reaction 2 and 3) is favored while the conversion to relatively linear units (products of idealized pyrolysis reaction 1) is inhibited (the hypothetical structure of the strands formed in the pure Ar or H_2-

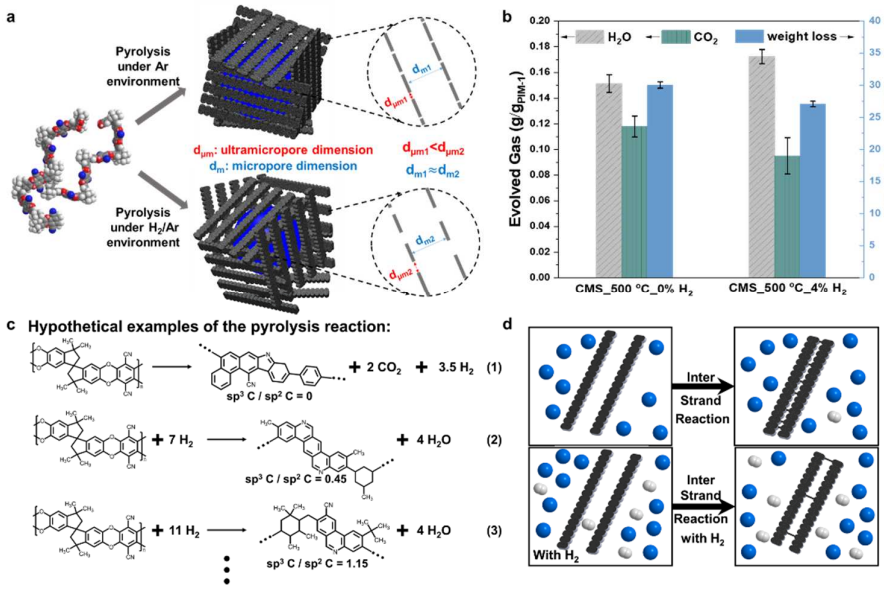

Figure 2. a) Illustration that the introduction of H_2 to the pyrolysis environment results in an enlargement of the ultramicropores with only minor changes in the size of the micropore. b) Quantitative results of the CO_2 and H_2O evolved from the pyrolysis processes measured by mass spectrometry along with the total sample weight loss after pyrolysis. c) Hypothetical example reaction pathways generating CO_2 and H_2O during pyrolysis; note that many pyrolytic reactions can be envisioned. d) Illustration of the effect of H_2 on the lateral linkages between strands. =H_2, =Ar.

included pyrolysis environment is shown in **Figure S3**). The carbonized strands are shorter and more mobile than the entangled precursor polymer, but must first "solve" a packing problem to maximize the entropy of the system. The rigid strands will organize into more easily packable plates (**Figure S1(iii)**) to have an overall higher entropy value and reduce the excluded volume present within a random phase packing of strands. The kinked structure generated in the presence of H_2 inhibits strand alignment (i.e., the "packing problem" will be more difficult to solve), which increases the imperfections within the plates of strands (details in the Supporting Information). This ultimately increases the sizes of the ultramicropores (discussed later).

It should be noted that lateral linkages between strands may occur due to inter-strand reactions, which can only evolve molecular H_2 in the process.[18a] However, the reaction between lateral stands will be suppressed by H_2 molecules present in the pyrolysis atmosphere thus resulting in reduced inter-strand crosslinking and larger gaps between the strands on average (as illustrated in **Figure 2d**). Kinetic restrictions (i.e., limited time for the final ramp and soak periods at high temperature) lead to the imperfect organization of strands within the plates themselves and long-range plate-stacking defects. A typical idealized micropore "cell" with imperfectly packed plates comprising imperfectly organized strands is illustrated in **Figure S1(iv)**. In CMS materials, the slits between strands are the ultramicropores that enable molecular sieving while the voids between the imperfectly-stacked plates are the micropores that provide abundant sorption sites and allow for guest molecules to realize many of their conformational degrees of freedom. During the soak and cooling phases, ongoing formation and coalescence (i.e., sharing ultramicroporous "walls" between cells) of multiple neighboring cells will generate an idealized CMS structure (**Figure S1(v)**) with a bimodal distribution of pores.

The tuning effect of H_2 on the pore structure of CMS is demonstrated by N_2 physisorption experiments performed at 77 K (**Figure S4** and **S5**). As illustrated in **Figure 3a and 3b**, three hydrogen volume fractions and a control experiment (i.e., 4, 2, 1, and 0 vol% H_2), were investigated using a final pyrolysis temperature of 500 °C. It is worth noting that reasonable nitrogen physisorption isotherms at 77 K for CMS pyrolyzed under a 0% H_2 atmosphere cannot be obtained, which indicates that the size of ultramicropores within this CMS is quite similar to N_2 (3.64 Å) thus resulting in extremely slow N_2 diffusion (it is important to note that these materials can still adsorb and permeate xylene isomers at 55°C).[11] In contrast, the CMS pyrolyzed under H_2-containing atmospheres revealed ultramicropores ranging from 5 to 7 Å, which are significantly larger than those in the CMS pyrolyzed without H_2. Moreover, the distributions of ultramicropores are narrower as the hydrogen content decreases from 4% to 1% (full width at half maximum decreases from 2.8 Å to 1.1 Å). Interestingly, the pore size distribution of the resulting CMS is similar to that of the PIM-1 precursor. It can be observed that the distributions of micropores do not change appreciably at the varying levels of hydrogen in the pyrolysis atmosphere. The micropores in CMS_500°C_0% H_2 are not detectable by N_2 physisorption experiments due to the extremely narrow ultramicropores existing in the sample. By comparing the pore size distribution of CMS samples pyrolyzed under 500 and 800 °C, one can see that higher pyrolysis temperature will narrow both the micropores and ultramicropores. As expected, under very high pyrolysis temperature (1100 °C), a severe tightening of the CMS matrix still occurs even in the presence of H_2. The above analysis indicates that both final pyrolysis temperature and H_2 concentration in the pyrolysis atmosphere play vital roles in the pore structure of CMS. Moreover, the development of these "mid-range" micropores is related to the polymer precursor structure. As a control experiment, we pyrolyzed Matrimid® (a high free volume polyimide, but not a PIM material) in the presence of H_2 and were unable to detect microporosity via N_2 physisorption techniques (**Figure S6**).

In order to investigate the carbon bonding nature inside the samples, each C1s spectrum from X-ray photoelectron spectroscopy (**Figure S7** and **S8**) for the different CMS samples is deconvoluted to three Gaussian peaks. For all the investigated samples, good fits were obtained as indicated by a square root of reduced χ^2 less than 3 and a coefficient of determination R^2 greater than 0.99. The two strongest signals with a relative binding energy distance of around 1 eV between their maxima are associated with different hybridization states.

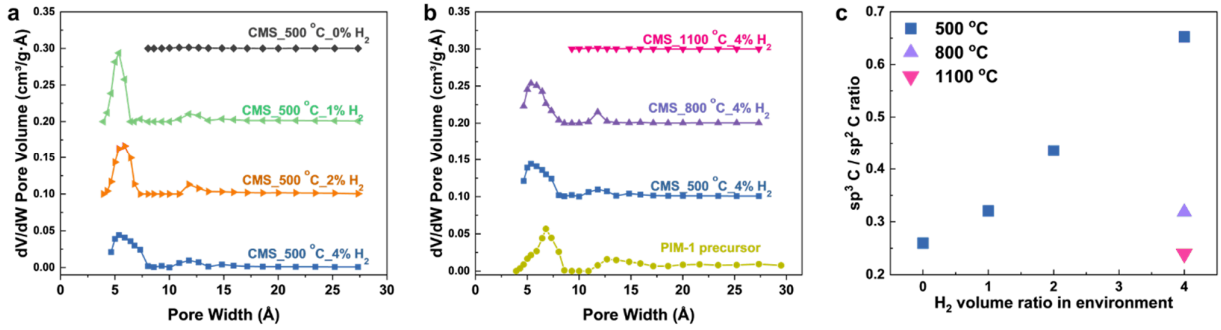

Figure 3. Pore size distributions measured by N_2 physisorption at 77 K for CMS pyrolyzed under a) different H_2 concentrations and b) different final pyrolysis temperatures. c) sp^3/sp^2 carbon ratio as a function of H_2 concentration determined from XPS spectra.

The lower binding energy signal corresponds to the sp^2-hybridized carbon, and the signal with an energy shift of around 1 eV higher is attributed to the sp^3 hybridized carbon.[19] Moreover, a third signal observed around 289 eV is evidence of the existence of a C-O carbon state.[20] On one hand, we hypothesize that sp^3 hybridized carbon, a three-dimensional structure, disrupts the plate packing and is useful for imparting high guest molecule flux. On the other hand, we hypothesize that sp^2 hybridized carbons, a two-dimensional graphite layered structure, enable plate packing and thus lead to more compact microstructures with smaller ultramicroporous gaps in the plates. Therefore, a higher ratio of sp^3/sp^2 carbons should result in more permeable, yet less selective structures. The sp^2 and sp^3 hybridized carbon content in each CMS sample can be estimated by their peak area ratios from the XPS spectra. As shown in **Figure 3c,** the sp^3/sp^2 carbon ratio in the CMS increased monotonically with a decrease in pyrolysis temperature or an increase in hydrogen concentration. The increased sp^3/sp^2 carbon ratio also implies a higher free volume, which is generally consistent with the N_2 physisorption results (**Table S2**). From X-ray diffraction (XRD) and Fourier transform infrared spectroscopy (FTIR), as shown in the Supporting Information, **Figure S9** and **S10**, the obtained CMS are highly disordered and amorphous carbon materials, similar to a previous report.[11]

The sorption isotherms of *p*-xylene and *o*-xylene collected at 55 °C for both CMS_500 °C_4% H_2 and CMS_500 °C_0% H_2 (**Figure 4a**) display a sharp increase in adsorption capacity in the low saturation region and then plateau at higher saturation values. As might be expected, the uptake for *p*-xylene and *o*-xylene at each relative pressure exhibited only minor differences (within 1 wt%) relative to each other due to their similar chemical nature, revealing an absence of a sorption-selective separation mechanism. It is worth noting that both isomers have nearly identical sorption isotherms with the ones obtained for CMS_500 °C_4% H_2 and CMS_500 °C_0% H_2, indicating little change in the sorption properties of the CMS materials after the introduction of H_2 to the pyrolysis environment. Combined with the N_2 physisorption results, this suggests that the larger micropore volume in the CMS is relatively unaffected by the presence of the reactive H_2 pyrolysis gas, which indicates that the primary effect of the H_2 is to interfere with the formation of the plates.

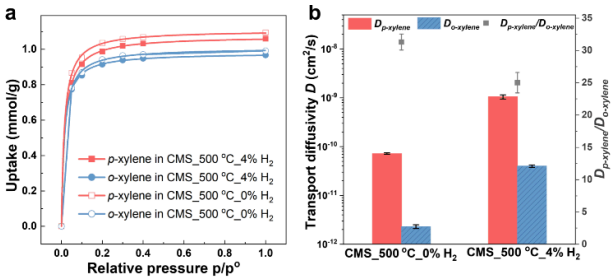

Figure 4. a) Single component sorption isotherms of *p*-xylene and *o*-xylene in CMS_500 °C_4% H_2 and CMS_500 °C_0% H_2 measured at 55 °C. b) Transport diffusion coefficients for xylene isomers in CMS_500 °C_4% H_2 and CMS_500 °C_0% H_2 at 55 °C.

The ultramicropores inside the rigid CMS enable molecular sieving and allow for more rapid activated diffusion of the smaller *p*-xylene molecules relative to the larger *o*-xylene molecules. Single component diffusion studies revealed significant differences in the kinetic uptakes (**Figure S11**) of *p*-xylene and *o*-xylene, with slower *o*-xylene diffusion observed, and these experiments were utilized to estimate the transport diffusivities, $\mathcal{D}$ (**Figure 4b**). The details of the organic solvent sorption measurements can be found in the Supporting Information. The transport diffusivities for both isomers in the H_2-pyrolyzed CMS samples increase significantly relative to the control case without H_2 in the pyrolysis environment (1.0×10^{-9} vs. 7.2×10^{-11} cm^2/s for *p*-xylene, 4.0×10^{-11} vs. 2.3×10^{-12} cm^2/s for *o*-xylene). Consistent with our observations of the ultramicropore size, the H_2-assisted CMS exhibits a slightly lower diffusion selectivity (25 vs. 31), which indicates that a trade-off between diffusion selectivity and diffusivity for CMS-type materials may exist.

The separation performance of the CMS membranes was tested using a Wicke-Kallenbach permeation setup, where the total pressure difference across the membrane is maintained at zero. The feed, either pure xylene or a xylene mixture vapor carried by nitrogen, flushes the upstream while a nitrogen sweep carries the permeate to a gas chromatograph to determine the xylene flux across the membrane (details in the Supporting Information). As illustrated in **Figure 5a** and **5b**, lower pyrolysis temperatures or higher H_2 concentration in the pyrolysis environment will result in a higher *p*-xylene permeability and a lower *p*-xylene/*o*-xylene permselectivity. It has been shown above that both the H_2 concentration and pyrolysis temperature effectively manipulate the pore size distribution and sp^3/sp^2 hybridized carbon ratio inside the CMS. As discussed previously, sp^3-hybridized carbon has a 3D structure that we hypothesize contributes to the molecular flux while sp^2-hybridized carbon is comprised of a planar structure. As noted earlier, we hypothesize that there might be a positive correlation between the sp^3/sp^2 hybridized carbon ratio of the CMS and the permeability of guest molecules. As shown in **Figure 5c**, as the sp^3/sp^2 hybridized carbon ratio increases from 0.24 to 0.65, the permeability of *p*-xylene through the CMS membranes improves significantly from 2.8×10^{-16} to 8.5×10^{-14} $mol\text{-}m/m^2\text{-}s\text{-}Pa$ (>300x, 30,257% increase) while the permselectivity decreases only slightly from 38.9 to 18.8 (52% decrease). To the best of our knowledge, this is the first study that has considered the correlation between the sp^3/sp^2 hybridized carbon ratio and the permeation properties of CMS membranes. This observation—if generalizable beyond the polymer and conditions investigated here—provides a fundamental basis for understanding and improving the separation performance of CMS membranes for various applications.

The effect of H_2 on the permeation performance of CMS membranes for the separation of xylene isomers is further illustrated in **Figure 5d** and **Figure S12** by the use of mixed xylene isomers feeds. Equimolar *p*-xylene/*o*-xylene vapor mixture permeation through dense membranes was also tested at 55 °C. **Figure S12** shows that tightening of the ultramicropores (via decreasing H_2 concentration or via increasing final pyrolysis temperature) improves the discrimination between xylene isomers at the cost of membrane permeability. As shown in **Figure 5d**, the membranes prepared at 4 vol% H_2/Ar gain at least 14 times more *p*-xylene permeability than the membrane prepared without H_2, as shown by estimates from the sorption-diffusion model and the experimental permeability from the Wicke-Kallenbach measurements. This is consistent with our characterization results that the larger ultramicropores generated with the help of H_2 provide less resistance to diffusion of guest molecules compared to the extremely narrow ultramicropores resulting from the pure Ar pyrolysis. Unlike the permeability, the permselectivity exhibits much smaller changes. This is likely owing to the fact that the permselectivity is mainly dominated by the ultramicropores inside the CMS membrane and the size of the H_2 enlarged ultramicropores is around 5-7 Å (note that the xylene isomers used, *p*-xylene and *o*-xylene, have kinetic diameters of 5.8 Å and 6.8 Å, respectively). As a result, the H_2-assisted CMS can still effectively distinguish between *p*-xylene and *o*-xylene via a kinetic effect provided by the rigid ultramicropores with the appropriate size. For the pure component Wicke-Kallenbach tests, the *p*-xylene permeability is higher and the permselectivity is lower than those predicted by the sorption-diffusion model (8.5×10^{-14} vs. 4.1×10^{-14} $mol\text{-}m/m^2\text{-}s\text{-}Pa$ and 18.8 vs. 24.6, respectively). This difference could be the result of some small, nonselective leak pathways inside or around the CMS membranes. The *p*-xylene permeability in the equimolar mixture test is smaller than the value obtained from the pure component test (6.0×10^{-14} vs. 8.5×10^{-14} $mol\text{-}m/m^2\text{-}s\text{-}Pa$) while the permselectivity decreases in the mixture case (14.7 vs. 18.8), which is a well-known " fingerprint" of the frictional coupling effects between rapidly and slowly transporting xylene molecules.

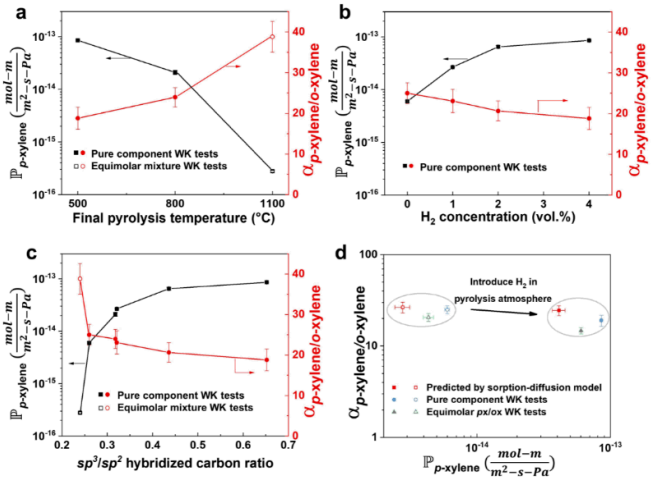

Figure 5. Permeation performance of dense CMS membranes at 55 °C. Permeability of *p*-xylene and permselectivity of *p*-xylene/*o*-xylene as a function of a) pyrolysis temperature, b) H_2 concentration in the pyrolysis environment and c) sp^3/sp^2 hybridized carbon ratio. d) *p*-Xylene/*o*-xylene separation performance of 4% H_2-assisted dense CMS membranes (solid markers) compared to Ar pyrolyzed membranes (hollow markers). Square: sorption-diffusion model predicted value, Circle: experimental data from pure component Wicke-Kallenbach tests, Triangle: experimental data from equimolar xylene vapor mixture Wicke-Kallenbach tests.

To demonstrate the ability of this concept to translate to the fabrication of membrane devices, we elected to pyrolyze defect-free PIM-1 hollow fiber membranes in the presence of 4% H_2 and at 500 °C. PIM-1 fiber pyrolyzed without H_2 is ultilized as a control case and its best performance is shown in **Table 1**.[21] In these experiments, both membranes are exposed to a fully saturated equimolar *p*-xylene and *o*-xylene vapor mixture, which simulates high activity liquid-phase organic solvent reverse osmosis conditions. As shown in **Table 1**, the permeation rate enhancements observed in the dense films are also observed for the fiber case. Specifically, CMS HFMs fabricated in an H_2-included pyrolysis environment exhibit increases of both permeance (~38x) and permselectivity (~6x; the anomalously low selectivity of the control case is not a result of defects and has been discussed elsewhere).[21] For a more direct comparison with state-of-the-art MFI-type zeolite membranes, the CMS HFMs fabricated in the H_2-included environment were also tested under a relatively low feed activity value (0.05), which is similar to the typical testing protocol for zeolitic membranes.[4] We observe that

Table 1. Separation results for PIM-1-derived CMS hollow fiber membranes.

Sample	Permeance ($10^{-11}\frac{mol}{m^2 \cdot s \cdot Pa}$)		Separation factor *p*X/*o*X	*p*X activity feed/ permeate	Relative saturation of feed/ permeate	Test mode
	*p*X	*o*X				
CMS_HFM_0%[a]	1.36 ± 0.04	0.98 ± 0.06	1.4 ± 0.1	0.5/0	100%/~0%	WK[c]
CMS_HFM_4%[b]	52.3 ± 0.7	5.87 ± 0.04	8.9 ± 0.2	0.5/0	100%/~0%	WK[c]
	222 ± 14	18.8 ± 0.5	11.8 ± 0.5	0.025/0	5%/~0%	WK[c]
	25.5[e] 36.0[f]	0.78[e] 0.21[f]	3.7	1.22/0.98[g]	100%/100%	OSRO[d]

[a] CMS pyrolyzed at 575 °C from previous work.[21]. [b] CMS pyrolyzed at 500 °C. [c] Wicke-Kallenbach tests were conducted at 55 °C with a nitrogen sweep on the permeate side with an equimolar *p*-xylene and *o*-xylene feed. [d] Organic solvent reverse osmosis tests were conducted at 22 °C under 60 bar with a 90:10 (mol/mol) mixture of *p*-xylene and *o*-xylene liquid feed and a stage cut of < 1%. The permeate composition was found to be 97.1 mol% *p*-xylene at steady state. [e] Hydraulic permeance based on the transmembrane pressure difference. [f] Intrinsic permeance based on fugacity driving force. [g] The detailed calculation of the feed and permeate activity is available in **Table S3**; the thermodynamic reference state is the pure liquid at 22 °C and 1 atm.

permeance increases significantly (~4.2x, to 2.2×10^{-9} $mol/m^2\text{-}s\text{-}Pa$) and permselctivity is improved to 11.8. Continued refinements of the pyrolysis atmosphere, protocol, and polymer precursors have the potential to make CMS membranes perform comparably with MFI for high activity solvent vapor separations (**Figure S13-15**).[4b, 22] Moreover, the hollow fiber CMS materials enable energy-efficient, liquid phase, osmotically-moderated separations that generally have much higher product fluxes and lower separation factors than MFI and CMS membranes operating in vapor separation modalities (**Table S3**). Our experimental OSRO results reveal that the separation performance of the PIM-1-derived CMS HFM was comparable to the cross-linked polyvinylidene fluoride (PVDF) derived CMS HFM described in earlier work[8]; importantly, the PIM-1 CMS HFM has a dramatically simplified fabrication scheme, which makes PIM-1-derived CMS more attractive for scale-up and practical applications.

In summary, the microstructure of PIM-1-derived CMS membranes is facilely tuned by the pyrolysis of polymer precursor in the presence of H_2. During the pyrolysis process, the introduction of H_2 inhibits aromatization of the decomposing polymer network. The size of the ultramicropores inside pure Ar pyrolyzed CMS is quite similar to N_2 while the CMS pyrolyzed under an H_2-included environment shows ultramicropores ranging from 5-7 Å, which fit the size of methyl-substituted benzene derivatives better (5.3-8.0 Å). The increase of H_2 concentration in the pyrolysis environment or the decrease of pyrolysis temperature results in an increase in ultramicropore size and sp^3/sp^2 carbon ratio, which we hypothesize is a fundamental property related to the transport properties of guest molecules in the CMS membrane. The H_2-assisted CMS membranes reveal good *p*-xylene/*o*-xylene separation with a significant increase in *p*-xylene permeability of 6.0×10^{-14} $mol\text{-}m/m^2\text{-}s\text{-}Pa$) and a *p*-xylene/*o*-xylene selectivity of 14.7 for equimolar mixture tests. Moreover, the hollow fiber CMS membranes, fabricated under 4% H_2/Ar show a *p*-xylene permeance of 5.2×10^{-10} $mol/m^2\text{-}s\text{-}Pa$ and a high activity vapor mixture permselectivity of 8.9 based on WK measurements and a *p*-xylene hydraulic permeance of 2.6×10^{-10} $mol/m^2\text{-}s\text{-}Pa$ and a separation factor of 3.7 based on OSRO tests. In general, this relatively rapid and straightforward pyrolysis method is expected to be further extended for the fabrication of CMS derived from other kinds of polymeric precursors and open up new opportunities for the membrane-based applications of CMS materials.

Acknowledgements

The authors thank ExxonMobil Research & Engineering for funding this research. The authors also thank Prof. William Koros, Prof. M.G. Finn, Dr. Dhaval Bhandari, Dr. JR Johnson, Dr. Benjamin McCool, and Dr. Daniel Zhou for their helpful discussions.

Conflict of interest

The authors declare no conflict of interest.

Keywords: carbon molecular sieve • hydrogen • membranes • polymer of intrinsic microporosity • xylene isomer separation

[1] a) D. S. Sholl, R. P. Lively, *Nature* **2016**, *532*, 435-438; b) S. Karan, Z. Jiang, A. G. Livingston, *Science* **2015**, *348*, 1347-1351.
[2] W. Yuan, Y. Lin, W. Yang, *J. Am. Chem. Soc.* **2004**, *126*, 4776-4777.
[3] a) M. Y. Jeon, D. Kim, P. Kumar, P. S. Lee, N. Rangnekar, P. Bai, M. Shete, B. Elyassi, H. S. Lee, K. Narasimharao, *Nature* **2017**, *543*, 690-694; b) M. S. Silva, A. E. Rodrigues, J. P. Mota, *AIChE J.* **2016**, *62*, 241-255.
[4] a) D. Kim, M. Y. Jeon, B. L. Stottrup, M. Tsapatsis, *Angew. Chem. Int. Ed.* **2018**, *57*, 480-485; b) Z. Lai, G. Bonilla, I. Diaz, J. G. Nery, K. Sujaoti, M. A. Amat, E. Kokkoli, O. Terasaki, R. W. Thompson, M. Tsapatsis, *Science* **2003**, *300*, 456-460.
[5] a) M. Daramola, A. Burger, M. Pera-Titus, A. Giroir-Fendler, L. Lorenzen, J.-A. Dalmon, *Sep. Sci. Technol.* **2009**, *45*, 21-27; b) G. Xomeritakis, S. Nair, M. Tsapatsis, *Micropor. Mesopor. Mater.* **2000**, *38*, 61-73.
[6] Y. Khabzina, C. Laroche, J. Perez-Pellitero, D. Farrusseng, *Micropor. Mesopor. Mater.* **2017**, *247*, 52-59.
[7] a) D. R. Paul, *Science* **2012**, *335*, 413-414; b) W. J. Koros, C. Zhang, *Nat. Mater.* **2017**, *16*, 289-297.
[8] D.-Y. Koh, B. A. McCool, H. W. Deckman, R. P. Lively, *Science* **2016**, *353*, 804-807.
[9] N. B. McKeown, P. M. Budd, *Chem. Soc. Rev.* **2006**, *35*, 675-683.
[10] a) O. Salinas, X. Ma, E. Litwiller, I. Pinnau, *J. Membr. Sci.* **2016**, *504*, 133-140; b) H. Yin, Y. Z. Chua, B. Yang, C. Schick, W. J. Harrison, P. M.

Budd, M. Böhning, A. Schönhals, *J. Phys. Chem. Lett.* **2018**, *9*, 2003-2008.

[11] Y. Ma, F. Zhang, S. Yang, R. P. Lively, *J. Membr. Sci.* **2018**, *564*, 404-414.

[12] a) J. Jang, B. Lim, *Adv. Mater.* **2002**, *14*, 1390-1393; b) R. Ryoo, S. H. Joo, M. Kruk, M. Jaroniec, *Adv. Mater.* **2001**, *13*, 677-681; c) J. Lee, S. Han, T. Hyeon, *J. Mater. Chem.* **2004**, *14*, 478-486.

[13] a) X. Ning, W. J. Koros, *Carbon* **2014**, *66*, 511-522; b) S. Fu, E. S. Sanders, S. S. Kulkarni, W. J. Koros, *J. Membr. Sci.* **2015**, *487*, 60-73.

[14] H. J. Kim, D.-G. Kim, K. Lee, Y. Baek, Y. Yoo, Y. S. Kim, B. G. Kim, J.-C. Lee, *Sci. Rep.* **2016**, *6*, 36078.

[15] P. M. Budd, E. S. Elabas, B. S. Ghanem, S. Makhseed, N. B. McKeown, K. J. Msayib, C. E. Tattershall, D. Wang, *Adv. Mater.* **2004**, *16*, 456-459.

[16] M. L. Jue, V. Breedveld, R. P. Lively, *J. Membr. Sci.* **2017**, *530*, 33-41.

[17] A. S. Gasse, Experimentelle Bestimmung und Simulation von Explosionsgrenzen, untersucht an wasserstoffhaltigen Brenngasgemischen, Dissertation, Uni-GH Paderborn, Germany, **1992**.

[18] a) M. Rungta, G. B. Wenz, C. Zhang, L. Xu, W. Qiu, J. S. Adams, W. J. Koros, *Carbon* **2017**, *115*, 237-248; b) J. S. Adams, A. K. Itta, C. Zhang, G. B. Wenz, O. Sanyal, W. J. Koros, *Carbon* **2019**, *141*, 238-246.

[19] a) A. Wollbrink, K. Volgmann, J. Koch, K. Kanthasamy, C. Tegenkamp, Y. Li, H. Richter, S. Kämnitz, F. Steinbach, A. Feldhoff, *Carbon* **2016**, *106*, 93-105; b) H. Richter, H. Voss, N. Kaltenborn, S. Kämnitz, A. Wollbrink, A. Feldhoff, J. Caro, S. Roitsch, I. Voigt, *Angew. Chem. Int. Ed.* **2017**, *56*, 7760-7763; c) P. Merel, M. Tabbal, M. Chaker, S. Moisa, J. Margot, *Appl. Surf. Sci.* **1998**, *136*, 105-110.

[20] J. F. Watts, *High resolution XPS of organic polymers: The Scienta ESCA 300 database*, (Eds.: G. Beamson and D. Briggs), John Wiley & Sons, Chichester, **1992**, pp. 280

[21] M. L. Jue, Y. Ma, R. P. Lively, *ACS Appl. Polym. Mater.* In press, Jul. **2019**.

[22] J. Hedlund, J. Sterte, M. Anthonis, A.-J. Bons, B. Carstensen, N. Corcoran, D. Cox, H. Deckman, W. De Gijnst, P.-P. de Moor, *Micropor. Mesopor. Mater.* **2002**, *52*, 179-189.